Studies on Thermoelectric Properties of n-type Polycrystalline SnSe[subscript 1-x]S[subscript x] by Iodine Doping

Citation: Zhang, Qian, Eyob Kebede Chere, Jingying Sun, Feng Cao, Keshab Dahal, Shuo Chen, Gang Chen, and Zhifeng Ren. "Studies on Thermoelectric Properties of N-Type Polycrystalline SnSe[subscript 1-x]S[subscript x] by Iodine Doping." Advanced Energy Materials 5, no. 12 (June 2015): n/a – n/a.

As Published: http://dx.doi.org/10.1002/aenm.201500360

Publisher: Wiley Blackwell

Persistent URL: http://hdl.handle.net/1721.1/99891

Version: Author's final manuscript: final author's manuscript post peer review, without publisher's formatting or copy editing

Studies on Thermoelectric Properties of n-type Polycrystalline $SnSe_{1-x}S_x$ by Iodine Doping

Qian Zhang,[a, #] Eyob Kebede Chere,[a, #] Jingying Sun,[a] Feng Cao,[a] Keshab Dahal,[a] Shuo Chen,[a] Gang Chen,[b] Zhifeng Ren[a*]

ABSTRACT

We prepared iodine-doped n-type SnSe polycrystalline by melting and hot pressing. The prepared material is anisotropic with a peak *ZT* of ~0.8 at about 773 K measured along the hot pressing direction. This is the first report on TE properties of n-type Sn chalcogenide alloys. With increasing content of iodine, the carrier concentration changed from 2.3×10^{17} cm^{-3} (p-type) to 5.0×10^{15} cm^{-3} (n-type) then to 2.0×10^{17} cm^{-3} (n-type). The decent *ZT* is mainly attributed to the intrinsically low thermal conductivity due to the high anharmonicity of the chemical bonds like those in p-type SnSe. By alloying with 10 atm. % SnS, even lower thermal conductivity and an enhanced Seebeck coefficient were achieved, leading to an increased *ZT* of ~1.0 at about 773 K measured also along the hot pressing direction.

Dr. Q. Zhang, E. K. Chere, J. Y. Sun, Dr. F. Cao, K. Dahal, Prof. S. Chen, Prof. Z. Ren

[a]Department of Physics and TcSUH, University of Houston, Houston, Texas 77204, USA

Email: zren@uh.edu

Prof. G. Chen

[b]Department of Mechanical Engineering, Massachusetts Institute of Technology, Cambridge, Massachusetts 02139, USA

Q.Z., and E.-K.C. contributed equally.

INTRODUCTION

Thermoelectric (TE) power generators enable the direct conversion from heat to electricity. Ideal materials for thermoelectric generators should possess high dimensionless figure of merit $ZT = [S^2\sigma/(\kappa_{e+}\kappa_L)]T$, where S, σ, κ_e, κ_L, and T are the Seebeck coefficient, electrical conductivity, electronic thermal conductivity, lattice thermal conductivity, and absolute temperature, respectively.[1] The exploration from metals to alloys and from single crystals to nanostructures pushed the *ZT* values higher and higher.[1-11] Many approaches, such as resonant doping[12, 13], band convergence[14, 15], all-scale hierarchical structure[16, 17], etc. have been realized in the group IV-VI semiconductors. Peak *ZT*s as high as 2 were obtained frequently in different lead chalcogenide alloys.[16, 18, 19] Concerns on toxicity of lead also inspired the study of lead-free tin chalcogenides.[20-31] All the tin chacogenides (SnTe, SnSe, and SnS) were proved to be topological insulators.[32-34] It has been reported that p-type In-doped SnTe has *ZT* value higher than 1.0.[20] A surprising record *ZT* ~2.6 at 923 K was recently reported in p-type SnSe single crystal along one of the crystallographic directions.[23] This material was scarcely studied as TE materials due to the large band gap ~0.9 eV.[35-39] The high *ZT* is solely attributed to the intrinsically ultralow thermal conductivity due to high anharmonicity of the chemical bonds.[23, 40, 41] Considering the large-scale applications and the poor mechanical properties in the layered single crystal SnSe (crystallized in the orthorhombic *Pnma* space group), SnSe polycrystals were then studied.[26] However, due to lowered electrical conductivity and higher thermal conductivity, the peak *ZT* value was significantly decreased to lower than 1 at about 800 K.[26] Many kinds of p-type dopants were tested to increase the carrier concentration and electrical conductivity, and best peak *ZT* of ~0.6 at about 750 K was achieved in Ag-doped polycrystalline SnSe.[27] SnS (crystallized in the orthorhombic *Pbmn* space group) has the similar layered structure with SnSe and even larger band gap ~1.21 eV.[35, 36, 38, 39, 42, 43] Potential application of this environmentally compatible and low-cost material was predicted by first principles calculation[44] and a *ZT* of ~0.6 at about 900 K was recently obtained in p-type Ag-doped SnS polycrystals.[29] However, there is no report on n-type tin chalcogenide alloys up to now.

In this paper, we successfully prepared anisotropic I-doped n-type SnSe polycrystals with the highest *ZT* of ~0.8 at about 773 K measured along the hot-pressing direction. Since SnS and SnSe form a continuous series of solid solution,[35] by alloying with SnS, the thermal conductivity

decreased and the Seebeck coefficient increased, leading to an increased peak *ZT* of ~1.0 at about 773 K for $SnS_{0.1}Se_{0.87}I_{0.03}$ polycrystals measured also along the hot-pressing direction.

EXPERIMENTAL SECTION

N-type iodine-doped polycrystalline SnSe, $SnSe_{0.9}S_{0.1}$, and $SnSe_{0.7}S_{0.3}$ were prepared by melting the raw materials (Sn granules, 99.9%; Se granules, 99.99%; S pieces, 99.999%; and SnI_2 beads, 99.99%) in the double sealed quartz tubes. The raw materials were slowly (100 $^oC\ h^{-1}$) raised to 920 ^oC and kept for 6 h, then slowly (100 $^oC\ h^{-1}$) cooled to 600 ^oC and stayed at that temperature for 70 h, finally slowly (100 $^oC\ h^{-1}$) cooled to room temperature. The obtained ingots were cleaned and sealed inside the jar in an argon filled glove box and broken down by a high-energy ball mill SPEX 8000D (SPEX Sample Prep.) for 1 min to get the powder. SnSe is anisotropic. High *ZT* was found in single crystal along one of the crystallographic directions, not all directions. High energy ball milling for long time will eliminate the anisotropy therefore we only used a very short milling time: 1 min, to achieve some anisotropy in the grains. The powder was loaded into the half-inch die and hot pressed by alternating current (ac-HP) press at 600 ^oC for 7 min under 50 MPa to get a 14 mm rod. Considering the anisotropy of SnSe and SnS, all the samples were cut from both parallel and perpendicular to the pressing direction and measured along both directions. X-ray diffraction spectra analysis was conducted on a PANalytical multipurpose diffractometer with an X'celerator detector (PANalytical X'Pert Pro) from different directions of the anisotropic sample. The lattice parameters were calculated by the Rietveld refinement method. The microstructures were investigated by a scanning electron microscope (SEM, LEO 1525) and a high resolution transmission electron microscope (HRTEM, JEOL 2000FX). The chemical composition was analyzed on an energy-dispersive X-ray (EDX) spectrometer attached to SEM (JEOL 6330F). Room temperature optical diffuse reflectance spectra of the powder were obtained on a UV-Vis-NIR Spectrophotometer (Cary 5000) equipped with a polytetrafluoroethylene (PTFE) integrating sphere. Absorption data were calculated from reflectance data using the Kubelka-Munk function. The optical band gaps were derived from absorption versus energy plots. The electrical resistivity (ρ) and Seebeck coefficient (S) were simultaneously obtained on a commercial system (ULVAC ZEM-3) from room temperature to 500 ^oC to avoid the effect of phase transition. The thermal conductivity κ was calculated using $\kappa = D\alpha C_p$, where *D* is volumetric density determined by the Archimedes

method, α the thermal diffusivity obtained on a laser flash apparatus (Netzsch LFA 457) for an half inch disk with thickness of < 1.5 mm, and C_p the specific heat measured on a differential scanning calorimetry thermal analyzer (Netzsch DSC 404 C). The Hall Coefficient R_H at room temperature was measured using a PPMS (Quantum Design Physical Properties Measurement System) with a magnetic field of -3 T and 3 T and an electrical current of 8 mA. The Hall carrier concentration n_H was calculated using $n_H = 1/(eR_H)$. The uncertainty for the electrical conductivity is 3%, the Seebeck coefficient 5%, the thermal conductivity 7% (comprising uncertainties of 4% for the thermal diffusivity, 5% for the specific heat, and 3% for the density), so the combined uncertainty for the power factor is 10% and that for *ZT* value is 12%. Error bars were only used in the *ZT* vs *T* figures to increase the readability of the curves.

RESULTS AND DISCUSSION

SnSe crystallizes in a layered structure with orthorhombic *Pnma* space group (PDF #32-1382) at room temperature.[29] Figure 1 shows the XRD patterns taken in the plane parallel to the hot pressing direction (a) and perpendicular to hot pressing direction (b). The calculated lattice parameters for undoped SnSe (a = 11.48 Å, b = 4.15 Å, and c = 4.43 Å) are consistent with the reported data.[23, 26] The obvious difference in diffraction intensity in (400) and (111) planes (The ratio of the integral intensity of peak (400) to peak (111) is 0.47 in figure (a) and 2.2 in figure (b) for undoped SnSe.) indicates the existence of anisotropy of the samples in agreement with the microstructure shown in SEM image (figure 2 (a)). All the peaks were indexed without any impurity in spite of the high concentration of iodine. A structure transition from orthorhombic (*Pnma*) to orthorhombic (*Cmcm*)[23, 26, 45] undergoes at about 780 K as shown in figure 3 that shows the temperature dependence of specific heat for $SnSe_{1-y}S_y$ (y = 0, 0.1, and 0.3). This transition was pushed to a higher temperature when SnSe is alloyed with some SnS.

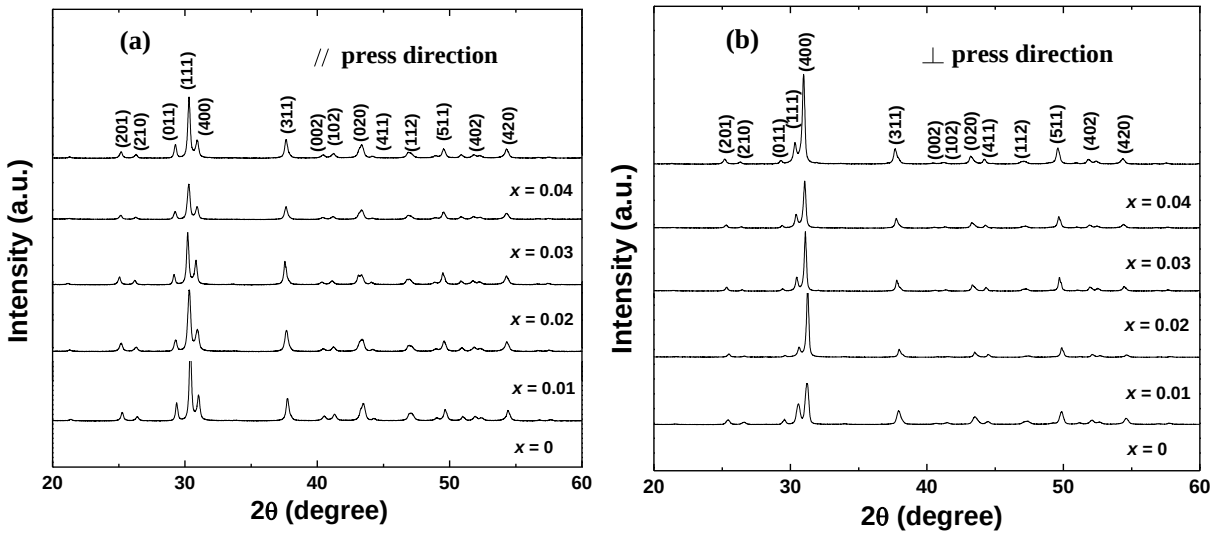

Figure 1. XRD patterns of bulk samples $SnSe_{1-x}I_x$ (x = 0, 0.01, 0.02, 0.03, and 0.04) (a) along the hot pressing direction and (b) perpendicular to the hot pressing direction.

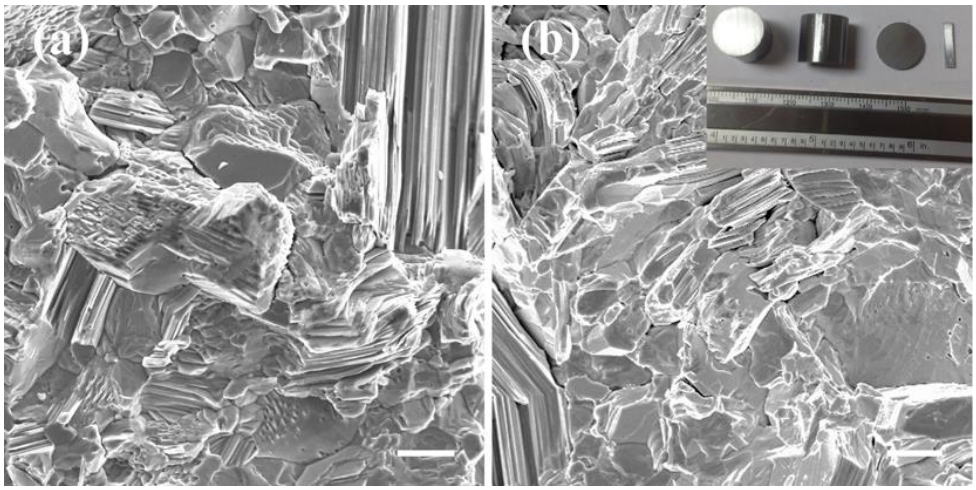

Figure 2. SEM fracture images of I-doped $SnSe_{0.97}I_{0.03}$ (a) on bulk samples perpendicular to the hot pressing direction and I-doped $SnSe_{0.87}S_{0.1}I_{0.03}$ (b) on bulk samples parallel to the hot pressing direction. The scale bar is 10 μm. Inset image: the hot pressed disk.

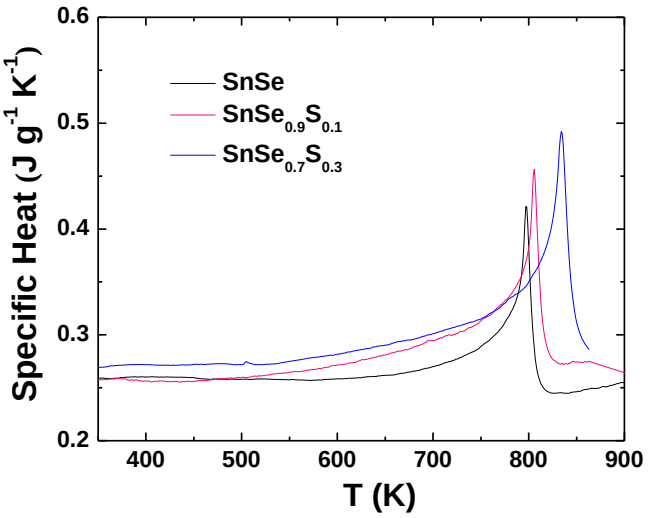

Figure 3. Temperature dependence of specific heat for $SnSe_{1-y}S_y$ (y = 0, 0.1, and 0.3). To be conservative, C_p of the undoped SnSe, $SnSe_{0.9}Se_{0.1}$, and $SnSe_{0.7}Se_{0.3}$ are used for the calculation of the total thermal conductivity of I-doped SnSe, $SnSe_{0.9}Se_{0.1}$, and $SnSe_{0.7}Se_{0.3}$, respectively. The small peak at about 500 K corresponds to the melting of maybe a very small amount of elemental Sn.[26]

The electrical conductivity of SnSe is much lower than those of the traditional state-of-the-art thermoelectric materials in spite of the single crystallization. The very high *ZT* of SnSe is attributed to the ultralow thermal conductivity due to the intrinsically high anharmonicity of the chemical bonds[23, 40]. Polycrystal SnSe has even lower electrical conductivity compared with single crystal SnSe.[26] The Hall carrier concentration can be increased from ~2×10^{17} cm^{-3} to ~9×10^{18} cm^{-3} by Ag doping.[27] However, the electrical conductivity is still low because of the low hole mobility in polycrystals. By doping with iodine, n-type SnSe polycrtstals were first prepared by melting and hot pressing in this study. Figure 4 shows the temperature dependence of electrical conductivity (a), Seebeck coefficient (b), power factor (c), thermal diffusivity (d), total thermal conductivity (e) and *ZT* (f) of all doped $SnSe_{1-x}I_x$ (x = 0.01, 0.02, 0.03, and 0.04) compared with undoped SnSe measured along the hot pressing direction. All the electrical conductivities increased with increasing temperature, showing typical semiconductor behavior. It has been reported that nominal stoichiometric SnSe shows p-type intrinsic behavior,[27] like the undoped result shown in figure 4. But actually it has real composition around $SnSe_{0.86}$ with Se

defect due to the evaporation of Se during melting and annealing (see table 1), but there is no Se evaporation after long time annealing (70 h) (see figure 3). If add up to 5 atm. % of extra Se when preparation, the compound still shows p-type with negligible carrier density change and become n-type with 5 atm. % extra Sn (but not stable).[27] In this study, iodine doping changed the conductive type from p to n in the whole temperature range when $x \geq 0.01$ confirmed by both the measured Seebeck coefficients and Hall coefficients (Figure 5) (The sample is also not stable when $x = 0.005$, showing p-type at room temperature as shown in figure 5 and n-type at higher temperature, not shown here). Both iodine doping and Sn overweight together created electrons, but the electron carrier density is limited to only $\sim 5 \times 10^{15}$ cm^{-3} for $x = 0.01$ and to $\sim 2 \times 10^{17}$ cm^{-3} for $x = 0.04$. The electrical conductivity decreased first ($x \leq 0.01$) then increased ($x \geq 0.01$) with increasing content of iodine, but the value is still as low as the undoped SnSe when $x = 0.04$. Thus in spite of the high Seebeck coefficient, the power factor is only ~4 μW cm^{-1} K^{-2} at about 800 K. Normally, Seebeck coefficient decreased with increasing carrier concentration. However, look at the Pisarenko relation for $SnSe_{1-x}I_x$ in figure 5 (b), the negative Seebeck coefficient increased with increasing electron carrier concentration when $x < 0.03$ due to the relatively high density of minority carriers when having too low electron carrier concentration. The high density of minority carriers decreased the Seebeck coefficient at low electron carrier concentration. Considering the low electronic thermal conductivity ($\kappa_e = L\sigma T$, where L is the Lorenz number), the lattice thermal conductivity ($\kappa_L = \kappa_{total} - \kappa_e$) is close to the total thermal conductivity shown in figure 4 (e). Similar with other reported SnSe,[23, 26, 27] high ZT ~0.8 at about 773 K as in figure 4 (f) is mostly benefit from this very low intrinsic thermal conductivity. We also show the properties of $SnSe_{0.97}I_{0.03}$ measured both parallel and perpendicular to the hot pressing direction in figure 6. The electrical conductivity and the thermal conductivity measured from perpendicular to the hot pressing direction are higher than those from parallel to the hot pressing direction and the Seebeck coefficient is almost the same from two directions. But the ZT is higher along the hot pressing direction.

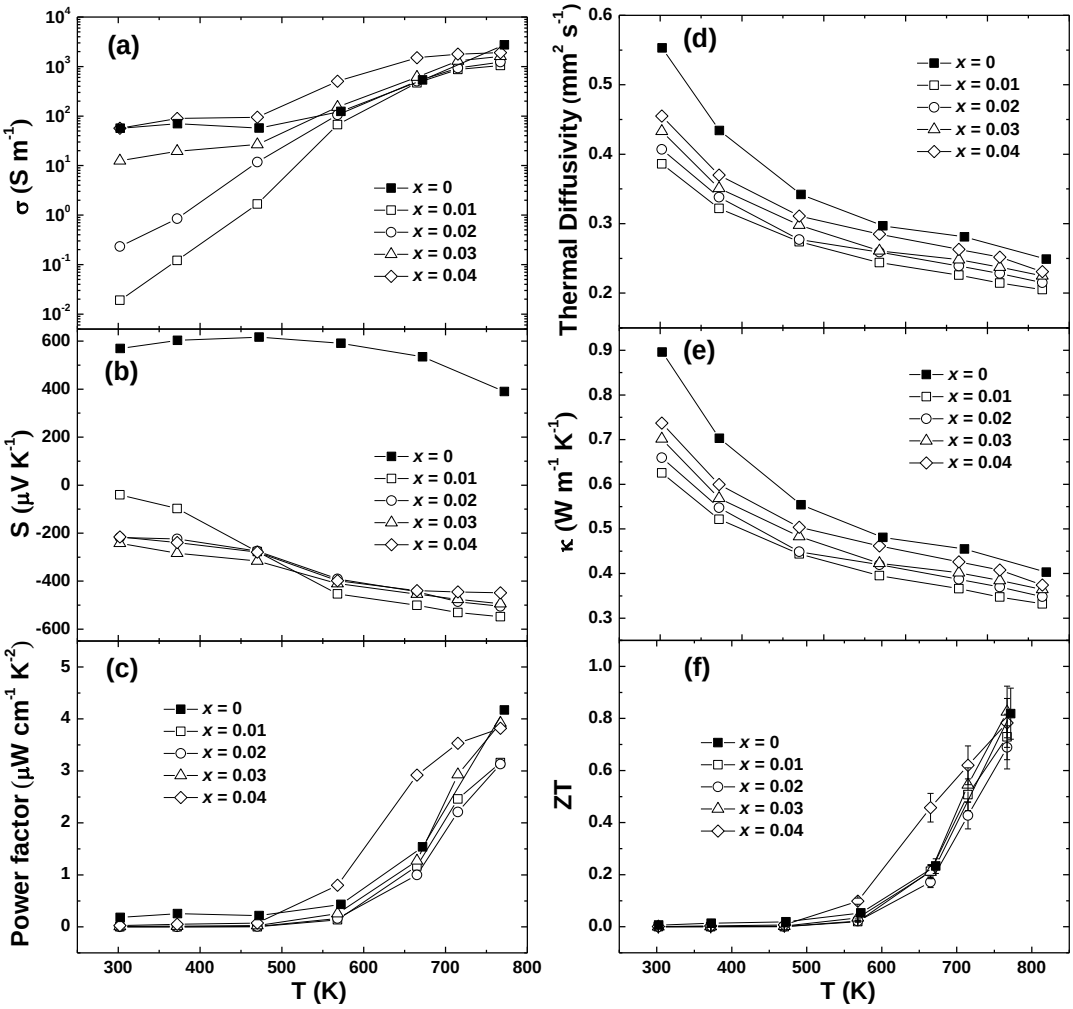

Figure 4. Temperature dependence of (a) electrical conductivity, (b) Seebeck coefficient, (c) power factor, (d) thermal diffusivity, (e) total thermal conductivity and (f) *ZT* for $SnSe_{1-x}I_x$ (x = 0, 0.01, 0.02, 0.03, and 0.04) measured along the hot pressing direction.

Table 1. Room temperature real composition, density, Hall carrier concentration, electrical conductivity, and total thermal conductivity for $SnSe_{1-x}I_x$ and $SnSe_{0.97-y}S_yI_{0.03}$.

Nominal Comp.	Real Comp.	Density (g cm^{-3})	n_H (10^{17} cm^{-3})	σ (S m^{-1})	κ (W m^{-1} K^{-1})
SnSe	$SnSe_{0.86}$	6.05	2.3	56.5	0.90
$SnSe_{0.995}I_{0.005}$	$SnSe_{0.891}I_{0.006}$	5.90	1.6	0.22	0.65
$SnSe_{0.99}I_{0.01}$	$SnSe_{0.883}I_{0.013}$	5.87	0.05	0.02	0.63

$SnSe_{0.98}I_{0.02}$	$SnSe_{0.856}I_{0.021}$	5.84	0.15	0.23	0.66
$SnSe_{0.97}I_{0.03}$	$SnSe_{0.884}I_{0.034}$	5.81	0.46	12.5	0.70
$SnSe_{0.96}I_{0.04}$	$SnSe_{0.873}I_{0.04}$	5.80	2.4	56.8	0.74
$SnSe_{0.87}S_{0.1}I_{0.03}$	$SnSe_{0.88}S_{0.07}I_{0.04}$	5.75	0.38	15.8	0.72
$SnSe_{0.67}S_{0.3}I_{0.03}$	$SnSe_{0.68}S_{0.29}I_{0.03}$	5.61	0.25	7.19	0.49

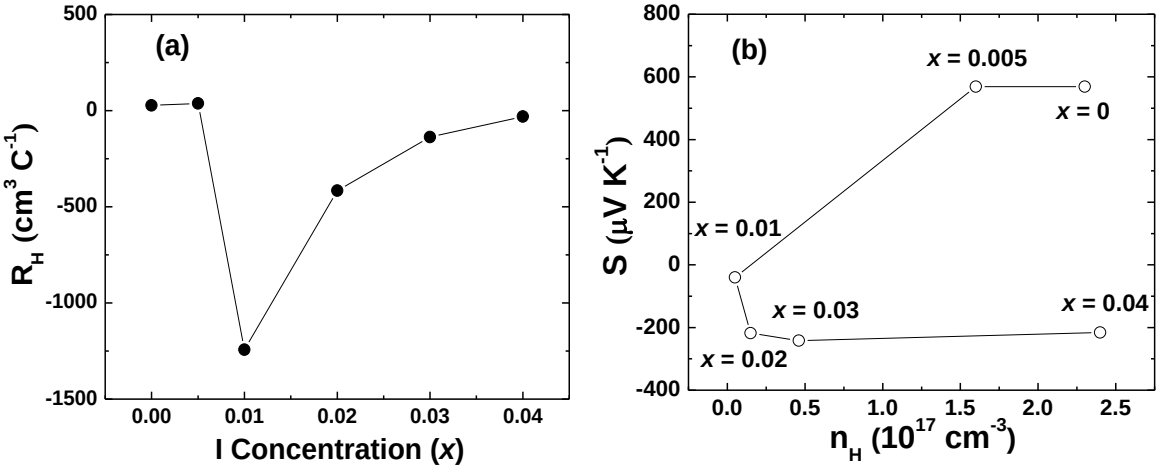

Figure 5. (a) Relationship between room temperature Hall coefficient (R_H) and iodine concentration (x) and (b) room temperature Pisarenko relation for $SnSe_{1-x}I_x$ (x = 0, 0.005, 0.01, 0.02, 0.03, and 0.04).

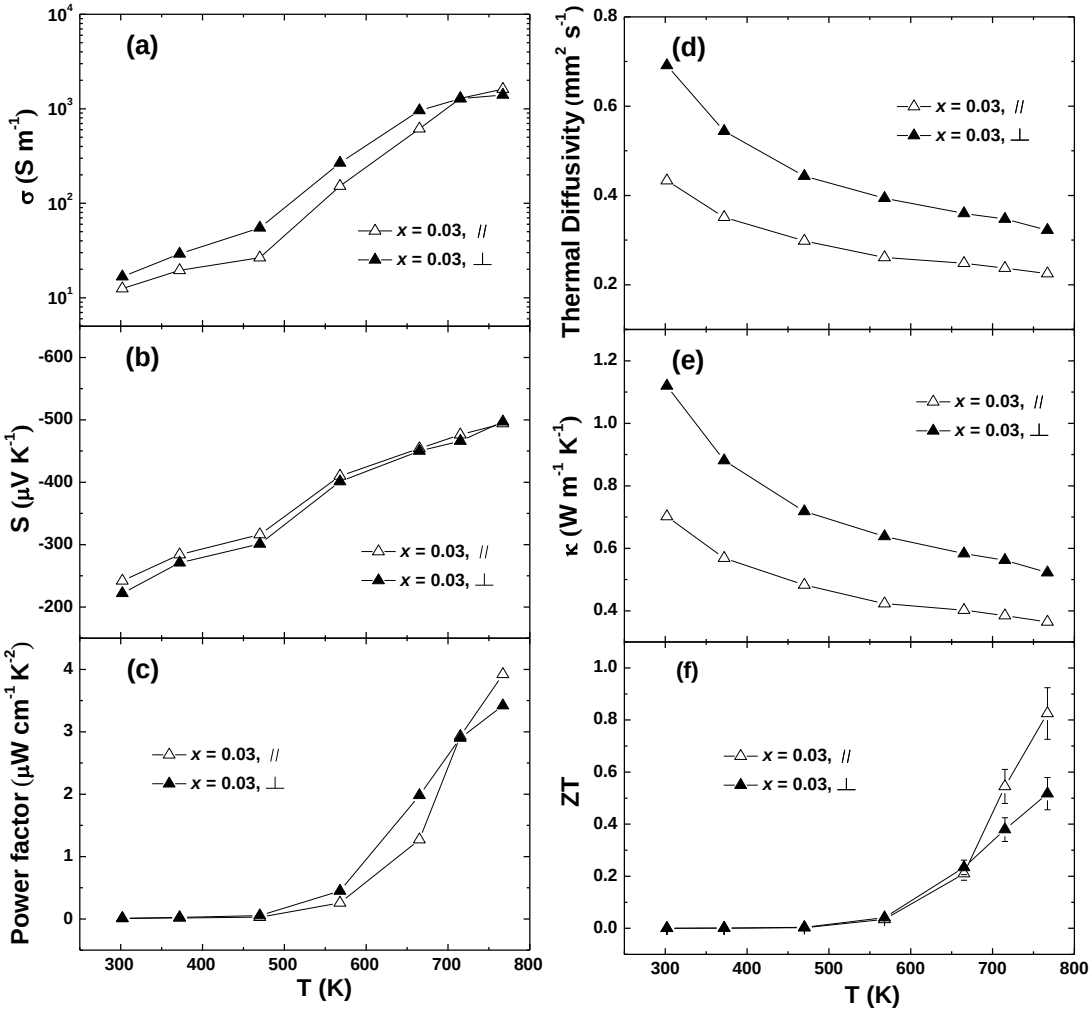

Figure 6. Temperature dependence of (a) electrical conductivity, (b) Seebeck coefficient, (c) power factor, (d) thermal diffusivity, (e) total thermal conductivity and (f) *ZT* for $SnSe_{0.97}I_{0.03}$ measured along the hot pressing direction (open symbols) and perpendicular to the hot pressing direction (filled symbols).

SnS also crystalizes in a layered structure with orthorhombic *Pbmn* space group (PDF #39-0354) at room temperature.[29] It undergoes the structure transition from orthorhombic to tetragonal at about 858 K.[29] We also studied the alloying effect of SnS into SnSe to see whether further reduction on thermal conductivity is possible. Figure 7 shows the XRD patterns of alloyed bulk samples $SnSe_{0.97-y}S_yI_{0.03}$ (y = 0, 0.1, and 0.3) parallel (a) and perpendicular (b) to hot pressing direction. Again we can see strong anisotropy in the samples, which is in consistent

with the SEM images presented in figure 2 (b). Because SnSe and SnS can form a continuous series of solid solutions, all the peaks of $SnSe_{0.97-y}S_yI_{0.03}$ were indexed to single phase with a minor right shift when SnS is increased. All the calculated lattice parameters (a, b and c) decreased with increasing concentration of SnS. Good solid solution is confirmed by good fitting to the Vegard's law in figure 2 (c).

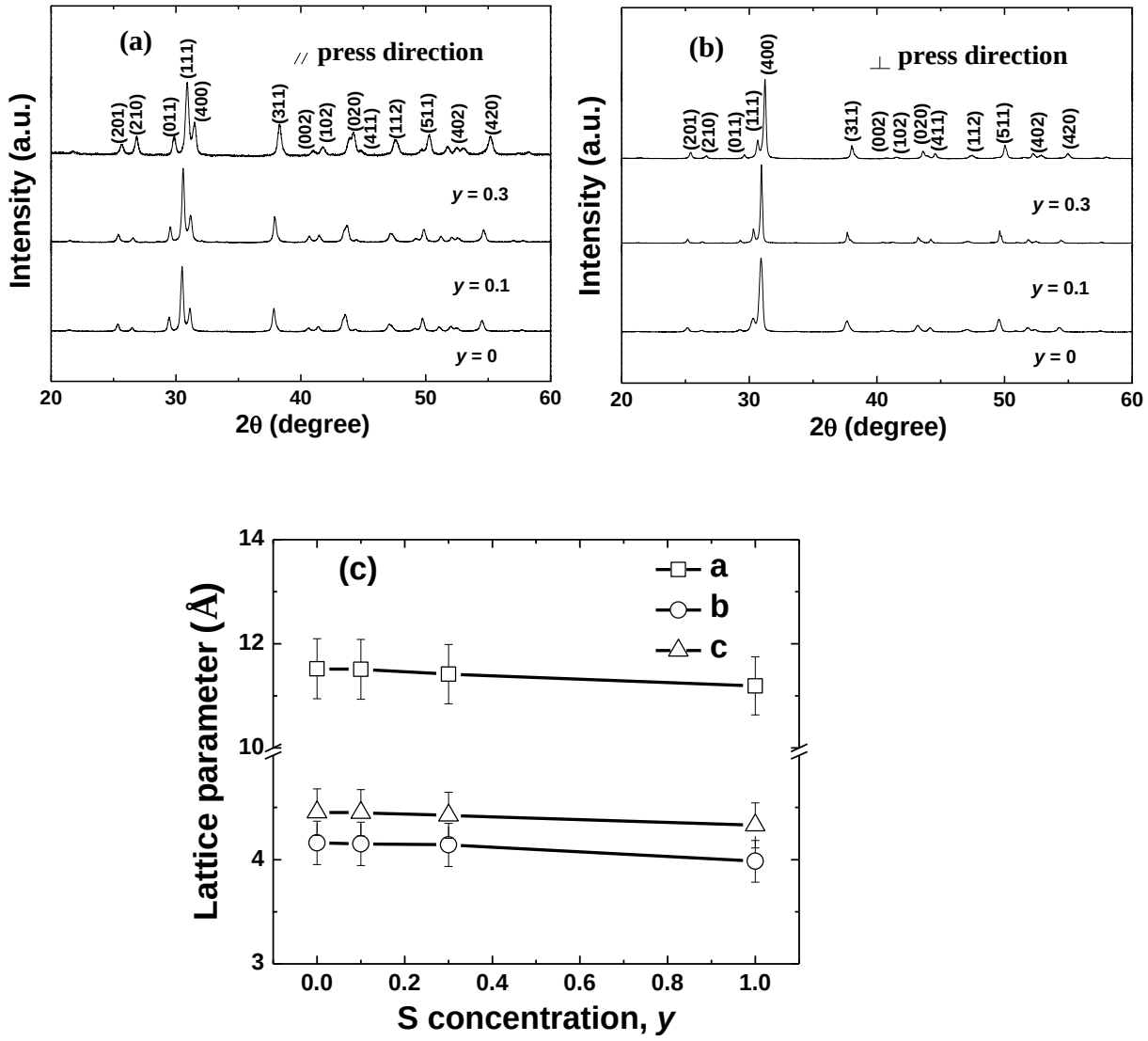

Figure 7. XRD patterns of bulk samples $SnSe_{0.97-y}S_yI_{0.03}$ (y = 0, 0.1, and 0.3) (a) along the hot pressing direction and (b) perpendicular to the hot pressing direction. The calculated lattice parameters were based on $SnSe_{0.97-y}S_yI_{0.03}$ (y = 0, 0.1, and 0.3). We use data from reference [29] for undoped SnS.

Figure 8 presents the temperature dependence of electrical conductivity (a), Seebeck coefficient (b), power factor (c), thermal diffusivity (d), total thermal conductivity (e) and *ZT* (f) of alloyed $SnSe_{0.97-y}S_yI_{0.03}$ (y = 0.1 and 0.3) compared with $SnSe_{0.97}I_{0.03}$ measured from along the hot pressing direction. Both the electrical conductivity and the thermal conductivity decreased with increasing content of SnS. Se evaporation was depressed and the electron carrier concentration decreased by introducing S (see table 1). Optical absorption spectra in figure 9 show that the band gap of undoped SnSe is ~0.94 eV, which is decreased to ~0.91 eV for $SnSe_{0.97}I_{0.03}$ by I doping and increased to ~0.97 eV for $SnSe_{0.67}S_{0.3}I_{0.03}$ and ~0.93 eV for $SnSe_{0.87}S_{0.1}I_{0.03}$ by alloying with SnS.

According to the Debye approximation, the theoretical lowest lattice thermal conductivity of the disordered crystals can be calculated as follows,[46]

$$k_{\min} = \left(\frac{\pi}{6}\right)^{1/3} k_B n^{2/3} \sum_i v_i \left(\frac{T}{\theta_i}\right)^2 \int_0^{\theta_i/T} \frac{x^3 e^x}{\left(e^x - 1\right)^2} dx \qquad (1)$$

where k_B is the Boltzmann constant, n is the atom numbers per volume, v_i and θ are the phonon velocity and Debye temperature for three sound modes (two transverse and one longitudinal), respectively. In our case, the calculated lowest lattice thermal conductivity is ~0.26 W m^{-1} K^{-1} at about 770 K for the low temperature orthorhombic (*Pnma*) phase SnSe, which is still lower than the experimental results for undoped (~0.4 W m^{-1} K^{-1}) and I-doped SnSe (~0.37 W m^{-1} K^{-1} for $SnSe_{0.97}I_{0.03}$) at 770 K shown in figure 4 (e). So although already having the very low thermal conductivity, we also tried alloying with SnS in 3 atm. % iodine-doped SnSe to further decrease the thermal conductivity. Due to the very low electrical conductivity, the lattice thermal conductivity is also close to the total thermal conductivity (figure 8 (e)), which showed decreasing close to the theoretical limit with more alloy scattering (~0.3 W m^{-1} K^{-1} for $SnSe_{0.87}S_{0.1}I_{0.03}$, and ~0.25 W m^{-1} K^{-1} for $SnSe_{0.67}S_{0.3}I_{0.03}$ at 770 K) (If more SnS alloyed, we should consider the theoretical limit of the $SnSe_{1-y}S_y$ alloys.). And they are close to the lattice thermal conductivity of the single crystals measured from b axis and c axis from 673 K-773 K[23]. The increased Seebeck coefficient by alloying, together with the lowered thermal conductivity kept the power factor at ~4 μW cm^{-1} K^{-2} and increased the highest *ZT* to ~1.0 at about 773 K for $SnSe_{0.87}S_{0.1}I_{0.03}$. This finding shows the first n-type Sn chalcogenide alloy also with decent peak *ZT*. However, we must notice the low average *ZT* of tin chalcogenides, even worse than that of

lead chalcogenides. Through the combination of nanostructures and complex band structure, an increased average *ZT* was obtained in Na-doped p-type PbTe/Ag_2Te (300-750 K).[47] Due to the stabilization of the optimal carrier concentration, an increase in average *ZT* was also achieved in Na-doped $Pb_{0.97}Mg_{0.03}Te$ (300-750 K).[48] Cr was recently found effective to increase the average *ZT*s of PbSe[49] and $PbTe_{1-x}Se_x$[50] (300-873 K). HgTe was recently used to enhance the low average *ZT* of SnTe (300-873 K).[30] Increased low temperature *ZT* could be expected in SnSe.

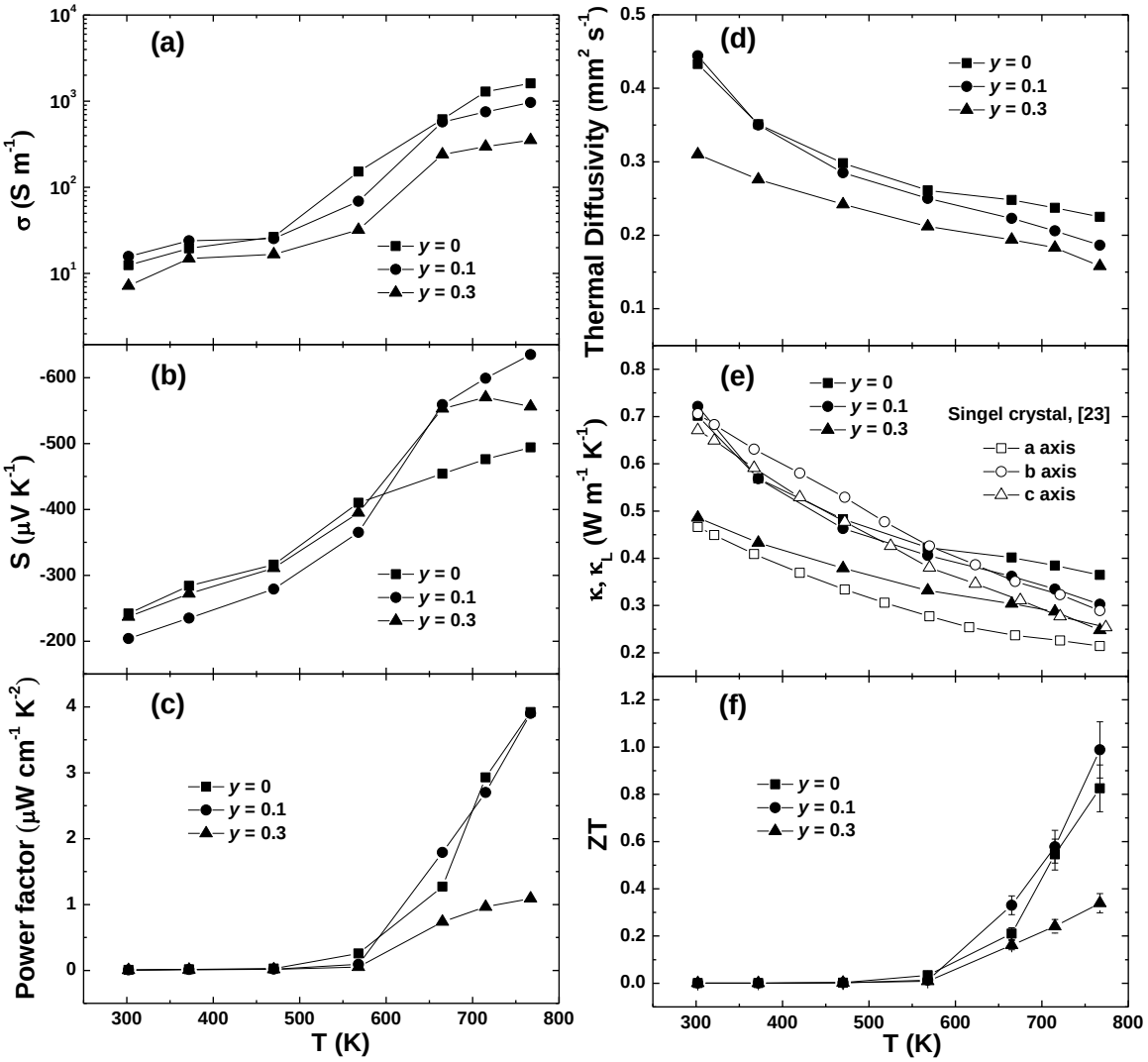

Figure 8. Temperature dependence of (a) electrical conductivity, (b) Seebeck coefficient, (c) power factor, (d) thermal diffusivity, (e) total thermal conductivity, and (f) *ZT* for $SnSe_{0.97-y}S_yI_{0.03}$ (y = 0, 0.1, and 0.3) measured along the hot pressing direction. The lattice thermal conductivity of the single crystal measured from different directions is plotted in (e) (open symbols) for

comparison[23]. Due to the very low electrical conductivity, the lattice thermal conductivity is very close to the total thermal conductivity in our study (solid symbols).

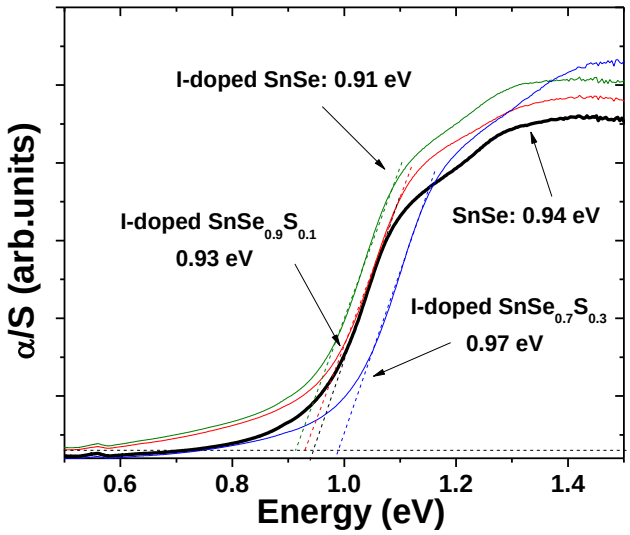

Figure 9. Optical absorption spectra and band gaps for undoped SnSe (black line), $SnSe_{0.97}I_{0.03}$ (green line), $SnSe_{0.87}S_{0.1}I_{0.03}$ (red line), and $SnSe_{0.67}S_{0.3}I_{0.03}$ (blue line).

CONCLUSIONS

I-doped n-type SnSe polycrystal was successfully prepared by melting and hot pressing. The electrons from iodine doping first decreased the hole carrier concentration and then increased the electron carrier concentration to ~2×10^{17} cm^{-3} in $SnSe_{0.96}I_{0.04}$. *ZT* of ~0.8 at about 773 K was obtained due to the intrinsic ultralow thermal conductivity in $SnSe_{0.97}I_{0.03}$. A higher *ZT* of ~1.0 at about 773 K was achieved by alloying 10 atm. % SnS with 3 atm. % I-doping due to even lower thermal conductivity. Although having potential peak *ZT*s (p-type: *ZT* = 2.6 at 923 K,[23] n-type: *ZT* = 1.0 at 773 K), to actually use this environmentally friendly and economic material, the average *ZT* needs to be increased.

ACKNOWLEDGEMENT: This work is supported by "Solid State Solar Thermal Energy Conversion Center (S^3TEC)", an Energy Frontier Research Center funded by the U.S. Department of Energy, Office of Science, Office of Basic Energy Science under award number DE-SC0001299.

REFERENCES

1 D. M. Rowe, *CRC Handbook of Thermoelectrics: Macro to nano* CRC Press, Taylor & Francis, Boca Raton, **2006**.

2 M. S. Dresselhaus, G. Chen, M. Y. Tang, R. G. Yang, H. Lee, D. Z. Wang, Z. F. Ren, J. P. Fleurial, P. Gogna, *Adv. Mater.* **2007**, *19*, 1043.

3 B. Poudel, Q. Hao, Y. Ma, Y. C. Lan, A. Minnich, B. Yu, X. Yan, D. Z. Wang, A. Muto, D. Vashaee, X. Chen, J. Liu, D. S. Dresselhaus, G. Chen, Z. F. Ren, *Science*, **2008**, *320*, 634.

4 B. C. Sales, D. Mandrus, R. K. Williams, *Science* **1996**, *272*, 1325.

5 D. Y. Chung, T. Hogan, P. Brazis, M. Rocci-Lane, C. Kannewurf, M. Bastea, C. Uher, M. G. Kanatzidis, *Science* **2000**, *287*, 1024.

6 A. Majumdar, *Science* **2004**, *303*, 777.

7 K. F. Hsu, S. Loo, F. Guo, W. Chen, J. S. Dyck, C. Uher, T. Hogan, E. K. Polychroniadis, M. G. Kanatzidis, *Science* **2004**, *303*, 818.

8 Y. Z. Pei, A. LaLonde, S. Iwanaga, G. J. Snyder, *Energy Environ. Sci*. **2011**, *4*, 2085.

9 A. D. LaLonde, Y. Z. Pei, G. J. Snyder, *Energy Environ. Sci* **2011**, *4*, 2090.

10 S. N. Guin, A. Chatterjee, D. S. Negi, R. Datta, K. Biswas, *Energy Environ. Sci.* **2013**, *6*, 2603.

11 S. N. Guin, V. Srihari, K. Biswas, *J. Mater. Chem. A* **2015**, *3*, 648.

12 J. P. Heremans, V. Jovovic, E. S. Toberer, A. Samarat, K. Kurosaki, A. Charoenphakdee, S. Yamanaka, G. J. Snyder, *Science* **2008**, *321*, 554.

13 Q. Y. Zhang, H. Wang, W. S. Liu, H. Z. Wang, B. Yu, Q. Zhang, Z. T. Tian, G. Ni, S. Lee, K. Esfarjani, G. Chen, Z. F. Ren, *Energy Environ. Sci.* **2012**, *5*, 5246.

14 Y. Z. Pei, X. Y. Shi, A. LaLonde, H. Wang, L. D. Chen, G. J. Snyder, *Nature* **2011**, *473*, 66.

15 Q. Zhang, F. Cao, W. S. Liu, K. Lukas, B. Yu, S. Chen, C. Opeil, G. Chen, Z. F. Ren, *J. Am. Chem, Soc*, **2012**, *134*, 10031.

16 K. Biswas, J. Q. He, I. D. Blum, C. I. Wu, T. P. Hogan, D. N. Seldman, V. P. Dravid, M. G. Kanatzidis, *Nature*, **2012**, *489*, 414.

17 Y. Lee, S. H. Lo, J. Androulakis, C. I. Wu, L. D. Zhao, D. Y. Chung, T. P. Hogan, V. P. Dravid, M. G. Kanatizidis, *J. Am. Chem, Soc*, **2013**, *135*, 5152.

18 R. J. Korkosz, T. C. Chasapis, S. H. Lo, J. W. Doak, Y. J. Kim, C. I. Wu, E. Hatzikraniotis, T. P. Hogan, D. N. Seidman, C. Wolverton, V. P. Dravid, M. G. Kanatzidis, *J. Am. Chem. Soc.* **2014**, *136*, 3225.

19 H. J. Wu, L. D. Zhao, F. S. Zheng, D. Wu, Y. L. Pei, X. Tong, M. G. Kanatizidis, J. Q. He, *Nat. Commun*. **2014**, *5*, 4515.

20 Q. Zhang, B. L. Liao, Y. C. Lan, K. Lukas, W. S. Liu, K. Esfarjani, C. Opeil, D. Broido, G. Chen, Z. F. Ren, *Proc. Natl. Acad. Sci. USA.* **2013**, *110*, 13261.

21 G. J. Tan, L. D. Zhao, F. Y. Shi, J. W. Doak, S. H. Lo, H. Sun, C. Wolverton, V. P. Dravid, C. Uher, M. G. Kanatzidis, *J. Am. Chem. Soc.* **2014**, *136*, 7006.

22 M. Zhou, Z. M. Gibbs, H. Wang, Y. Han, C. N. Xin, L. F. Li, G. J. Snyder, *Phys. Chem. Chem. Phys.* **2014**, DOI: 10.1039/c4cp02091j.

23 L. D. Zhao, S. H. Lo, Y. S. Zhang, H. Sun, G. J. Tan, C. Uher, C. Wolverton, V. P. Dravid, M. G. Kanatzidis, *Nature* **2014**, *508*, 373.

24 J. P. Heremans, *Nature* **2014**, *508*, 327.

25 H. Zhang, D. V. Talapin, *Angew. Chem. Int. Ed.* **2014**, *53*, 9126.

26 S. Sassi, C. Candolfi, J. B. Vaney, V. Ohorodniichuk, P. Masschelein, A. Dauscher, B. Lenori, *Appl. Phys. Lett.* **2014**, *104*, 212105.

27 C. L. Chen, H. Wang, Y. Y. Chen, T. Day, G. J. Snyder, *J. Mater. Chem. A* **2014**, *2*, 11171.

28 A. Banik, K. Biswas, *J. Mater. Chem. A* **2014**, *2*, 9620.

29 Q. Tan, L. D. Zhao, J. F. Li, C. F. Wu, T. R. Wei, Z. B. Xing, M. G. Kanatzidis, *J Mater. Chem. A* **2014**, *2*, 17302.

30 G. J. Tan, F. Y. Shi, J. W. Doak, H. Sun, L. D. Zhao, P. L. Wang, C. Uher, C. Wolverton, V. P. Dravid, M. G. Kanatzidis, *Energy Environ. Sci.* **2015**, *8*, 267.

31 A. Banik, U. S. Shenoy, S. Anand, U. V. Waghmare, K. Biswas, *Chem. Mater.* **2015**, *27*, 581.

32 T. H. Hsieh, H. Lin, J. Liu, W. H. Duan, A. Bansil, L. Fu, *Nature Commun.* **2012**, *3*, 982.

33 Y. Tanska, Z. Ren, T. Sato, K. Nakayama, S. Souma, T. Takahashi, K. Segawa, Y. Ando, *Nature Phys.* **2012**, *8*, 800.

34 Y. Sun, Z. C. Zhong, T. Shirakawa, C. Franchini, D. Z. Li, Y. Y. Li, S. Yunoki, X. Q. Chen, *Phys. Rev. B* **2013**, *88*, 235122.

35 W. Albers, C. Haas, H. Ober, G. R. Schodder, J. D. Wasscher, *J. Phys. Chem. Solids* **1962**, *23*, 215.

36 J. D. Wasscher, W. Albers, C. Haas, *Solid-State Electron.* **1963**, *6*, 261.

37 J. G. Yu, A. S. Yue, O. M. Stafsudd, *J. Cryst. Growth* **1981**, *54*, 248.

38 M. Parenteau, C. Carlone, *Phys. Rev. B* **1990**, 41, 5227.

39 B. B. Nariya, A. K. Dasadia, M. K. Bhayani, A. J. Patel, A. R. Jani, *Chalcogenide Lett.* **2009**, *6*, 549.

40 S. Lee, K. Esfarjani, T. F. Luo, J. W. Zhou, Z. T. Tian, G. Chen, *Nat. Commun.* **2014**, *5*, 3525.

41 G. J. Snyder, E. S. Toberer, *Nature Mater.* **2008**, *7*, 105.

42 W. Albers, C. Haas, H. J. Vink, J. D. Wasscher, *J Appl. Phys.* **1961**, *32*, 2220.

43 M. M. Nassary *J Alloy Comp.* **2005**, *398*, 21.

44 C. Bera, S. Jacob, I. Opahle, N. S. H. Gunda, R. Chmielowski, G. Dennler, G. K. H. Madsen, *Phys. Chem. Chem. Phys.* **2014**, *16*, 19894.

45 T. Chattopadhyay, J. Pannetier, H. G. Vonschnering, *J. Phys. Chem. Solids* **1986**, *47*, 879.

46 D. G. Cahill, S. K. Watson, R. O. Pohl, *Phys. Rev. B* **1992**, *46*, 6131.

47 Y. Z. Pei, A. H. Nicholas, A. LaLonde, G. J. Snyder, *Energy Environ. Sci.* **2011**, *4*, 3640.

48 Y. Z. Pei, A. D. LaLonde, N. A. Heinz, X. Y. Shi, S. Iwanaga, H. Wang, L. D. Chen, G. J. Snyder, *Adv. Mater.* **2011**, *23*, 5674.

49 Q. Zhang, E. K. Chere, K. McEnaney, M. L. Yao, F. Cao, Y. Z. Ni, S. Chen, C. Opeil, G. Chen, Z. F. Ren, *Adv. Enery Mater.* **2015**, 10.1002/aenm.201401977.

50 E. K. Chere, Q. Zhang, K. McEnaney, M. L. Yao, F. Cao, J. Y. Sun, S. Chen, C. Opeil, G. Chen, Z. F. Ren, *Nano Energy* **2015**, 10.1016/j.nanoen.2015.02.026.